ARTICLE   OPEN

Check for updates

Idarubicin combats abiraterone and enzalutamide resistance in prostate cells via targeting XPA protein

Ying Zhang[1,7], Wei Wei[2,7], Changying Li[3], Siyuan Yan[1], Shanshan Wang[1], Shudong Xiao[1], Chenchen He[4], Jing Li[5], Zhi Qi[5], Benyi Li [6], Kuo Yang [3]✉ and Changlin Li[1,3]✉

Although second-generation therapies like abiraterone (ABI) and enzalutamide (ENZ) benefit patients with castration-resistant prostate cancer (CRPC), drug resistance frequently occurs, eventually resulting in therapy failure. In this study, we used two libraries, FDA-approved drug library and CRISP/Cas9 knockout (GeCKO) library to screen for drugs that overcome treatment resistance and to identify the potential drug-resistant genes involved in treatment resistance. Our screening results showed that the DNA-damaging agent idarubicin (IDA) overcame abiraterone and enzalutamide resistance in prostate cancer cells. IDA treatment inhibited the DNA repair protein XPA expression in a transcription-independent manner. Consistently, XPA knockout sensitized prostate cancer cells to abiraterone and enzalutamide treatment. In conclusion, IDA combats abiraterone and enzalutamide resistance by reducing XPA protein level in prostate cancer.

INTRODUCTION

Prostate cancer is a leading cause of cancer-related death in Western countries. Androgen deprivation therapy (ADT) remains the standard treatment for prostate cancer patients who cannot undergo prostatectomy. Although ADT initially provides a potent benefit for patients with prostate cancer, their disease state inevitably progresses to castration-resistant prostate cancer (CRPC) within 2–3 years [1]. Abiraterone (ABI) and enzalutamide (ENZ) are second-generation therapies used for patients with CRPC [2–5]. Although both Abiraterone and enzalutamide have demonstrated clinical benefits [3, 4, 6], therapeutic resistance is common, limiting their clinical benefits and resulting in therapy failure after 6 months of treatment [7]. In addition, some patients with CRPC do not respond to abiraterone or enzalutamide treatment, indicating primary resistance [8]. The percentage of abiraterone primary resistance was approximately 10% and 40% in patients with and without chemotherapy, respectively [4, 5]. Similarly, 10% of chemotherapy-naïve patients with CRPC showed enzalutamide primary resistance, whereas 20% of patients pretreated with chemotherapy displayed enzalutamide primary resistance [6, 9]. Therefore, therapeutic resistance is a significant obstacle in CRPC patients. The development of therapeutic strategies to overcome biraterone and enzalutamide resistance is urgently needed [10].

DNA damage response (DDR) is an attractive therapeutic target for CRPC [11–13]. This may be due to the following reasons: (1) most patients with CRPC have DNA damage repair alterations and depend on the remaining DNA repair pathway for survival [14–16]. Therefore, targeting the remaining DNA repair pathways exhibits greater anti-cancer efficacy, leading to prolonged survival of DDR defected patients via the synthetic lethality approach [17]; (2) androgen receptor (AR) signaling pathway remains active in CRPC or ABI/ENZ-resistant patients, which activates the transcriptional expression of several DDR-related proteins in prostate cancers [18, 19]. The human gene XPA encodes a zinc finger protein acting as a DNA damage recognition and repair factor. XPA protein is an essential member of the nucleotide excision repair (NER) complex, a specialized DNA repair mechanism for UV radiation- and chemotherapeutic drugs-induced DNA damage [20–22]. Accumulating evidence showed that XPA protein is closely associated with chemotherapy and radiotherapy resistance in cancer patients [20]. Higher XPA expression is usually associated with poor prognosis in multi-types of human cancers [23], representing a potential target for anti-cancer therapy [20].

Idarubicin (IDA) is an anthracycline that exhibits potent antitumor activity against leukemia, including acute myeloid leukemia and acute promyelocytic leukemia [24]. In addition, clinical studies have indicated that IDA treatment benefits patients with hepatocellular carcinoma [25, 26]. In this study, we identified IDA as a candidate drug to combat ABI/ENZ resistance using a Food and Drug Administration (FDA)-approved drug library. Furthermore, we also determined that XPA is an essential target gene of IDA using liquid chromatography with tandem mass spectrometry (LC-MS/MS) proteomic analysis and the CRISPR-Cas9

knockout (GeCKO) library. Furthermore, in this study, we illustrated how IDA regulates the expression of XPA.

RESULTS
Idarubicin combats abiraterone resistance in prostate cancer cells
To screen for abiraterone-sensitizing drugs, abiraterone-resistant LNCaP cells (LNCaP/ABI) were treated with an FDA-approved drug library containing 1,815 drugs in duplicate (Fig. S1A, B and Supplemental Table S1). Drugs with more than 50% inhibition in duplicates were considered positive hits. Using this criterion, six drugs (i.e. Otilonium, Idarubicin, Auranofin, Sitafloxacin, Pyrvinium pamoate, and Erdafitinib) were identified as the positive hits from LNCaP/ABI screening (Fig. 1A and Supplemental Table S2). We then tested these candidates in two additional abiraterone-resistant prostate cancer cell lines, 22RV1/ABI and C4-2/ABI, as a secondary screening approach. Idarubicin (IDA) was identified as the only drug that inhibited the growth of all abiraterone-resistant cell lines (Fig. 1B). This inhibitory efficacy was confirmed in the parental and abiraterone-resistant subline cells(LNCaP/ABI, 22RV1/ABI, and C4-2/ABI), their parental control cell lines (LNCaP, 22RV1, and C4-2) (Fig. 1C, D, E), and RWPE-1 cells (Fig. 1F). The values for the 50% inhibition of cell growth (IC_{50}) were determined by Cell Counting Kit-8 (CCK-8) assay. The highest IC_{50} values were found in prostate epithelial RWPE-1 cells (Fig. 1G, I). The values for IC_{50} were significantly lower in the parental control cells than in abiraterone-resistant cells (Fig. 1H, I).

To further evaluate IDA inhibition of prostate cancer cell growth, the cell death assay was determined by Hoechst/PI staining. IDA treatment largely enhanced cell death in abiraterone-resistant cells, especially when abiraterone was added together with IDA (Fig. S2). These data indicate that Idarubicin (IDA) is the bona-fade candidate drug to combat Abiraterone resistance in castration-resistant prostate cancer cells.

To examine the in vivo antitumor effect of IDA on abiraterone-resistant prostate cancer, we established subcutaneous xenograft models in nude mice using LNCaP/ABI cells (Fig. 2A). IDA alone or in combination with abiraterone acetate (AA) treatment significantly reduced tumor growth (Fig. 2B) and prolonged mouse survival (Fig. 2C), while AA alone treatment had no obvious effect on tumor growth and animal survival. There were no significant changes in animal body weight among different treatment groups (Fig. 2D). Tissue examination by H&E staining showed no obvious abnormalities from major organs (Fig. S3). We also examined the antitumor effect of IDA on parental LNCaP-derived xenografts. LNCaP-derived mice were treated as described in Fig. 1A. LNCaP-derived xenografts were sensitive to AA treatment, and a combination of AA plus IDA treatments (Fig. 2E). These data indicated that IDA was effective in suppressing xenograft tumor growth without toxicity.

XPA combats abiraterone resistance in prostate cancer cells
To illustrate the mechanism underlying IDA-induced sensitization of abiraterone resistance, we analyzed the alterations of cellular protein levels in LNCaP/ABI cells after abiraterone plus IDA treatment for 24 h. Mass spectrometry-based protein profiling revealed that 519 proteins were lost in the combination treatment of abiraterone and IDA compared to the abiraterone treatment (Supplemental Table S3). Among these lost proteins, 87 proteins were ubiquitinated proteins, 60 proteins were mitochondrial localized, 55 proteins were zinc finger proteins, 35 proteins were involved in cell cycle modulation, 33 proteins were related to ubiquitination modulation, and 20 proteins were related to DNA damage repair (Supplemental Table S4).

To determine the critical genes involved in the progression of abiraterone resistance, LNCaP/ABI cells were infected with the GeCKO library and injected subcutaneously into the flanks of 8-week-old castrated male nude mice. When tumors were ~50 mm^3, mice were administered a dosage of AA (0.5 mmol/kg, every day). When tumors reached 1000 mm^3, they were removed from the mice and subjected to next-generation sequencing (NGS) (Fig. S4A). The curve of the cumulative frequency of sgRNAs after AA treatment shifted toward the left compared with the sgRNA cumulative frequencies before AA treatment (Fig. S4B). CRISPR/Cas9 screening data in this study were obtained from the Sequence Read Archive (SRA) at PRJNA780179. The Venn diagram shows that the expression of 11 genes, including XPA, involved in the development of abiraterone resistance, was decreased by IDA treatment (Fig. S4C and Table S5).

XPA is a potential drug target for tumor therapy. Therefore, we hypothesized that IDA overcomes abiraterone resistance by inhibiting XPA expression. To test this hypothesis, we first examined XPA expression after abiraterone treatment with or without IDA addition in resistant cells (LNCaP/ABI and 22RV1/ABI) and their parental control cell lines (LNCaP and 22RV1). IDA treatment largely reduced XPA protein levels in abiraterone-resistant cells but not their parental cells (Fig. 3A, B). Tumors from LNCaP/ABI-bearing mice treated with the combination of IDA and AA consistently displayed lower XPA expression compared with only IDA or DMSO treatment (Fig. 3C).

We next detected the effects of IDA treatment on DNA damage and AR expression in abiraterone-resistant cells. Both IDA alone and in combination with abiraterone treatment induced a drastic increase of γH2X protein, a DNA damage marker (Fig. 3D). AR protein expression did not change after treatment with these two agents (Fig. 3D). These data indicate that IDA inhibited the expression of XPA independent of the AR pathway, and XPA specifically targets IDA in abiraterone-resistant prostate cancer cells.

To verify the critical role of XPA reduction in overcoming abiraterone resistance, we knocked out the XPA gene using the CRISPR/Cas9 approach in abiraterone-resistant cell lines. LNCaP/ABI cells infected with sgSCR or sgXPA lentivirus were used to establish subcutaneous xenografts in nude mice (Fig. 3E). The combination of XPA knockout with AA treatment significantly inhibited tumor growth (Fig. 3F) and prolonged mouse survival (Fig. 3G) compared with the control sgSCR and AA alone treatment. To exclude the off-target effect of sgRNA on XPA, we knocked down XPA using anti-XPA shRNA in abiraterone-resistant cells. Consistent with the results of the XPA knockout using sgRNA for XPA, the knockdown of XPA significantly decreased cell viability in LNCaP/ABI (Fig. S5A, B). These data confirmed that XPA reduction is critical for IDA-induced abiraterone sensitization.

To further verify the role of XPA in abiraterone resistance, we then analyzed clinical profiles of XPA in prostate cancer using the TCGA database. A significantly higher level of XPA mRNA expression was seen in prostate cancer compared to that of control (Fig S6A). Furthermore, we then performed prognostic analysis for abiraterone-treated patients using the dataset (prad_su2c_2019) [27]. Kaplan-Myer survival analysis showed that higher XPA expression was significantly associated with worse overall survival (OS) in abiraterone-treated patients (Fig. S6B). These data suggest that XPA expression is negatively associated with the prognosis of abiraterone-treated patients with CRPC.

IDA treatment enhances XPA protein degradation through the proteasome pathway
To understand how IDA treatment reduces XPA expression, we first analyzed XPA mRNA expression after IDA treatment. IDA alone and in combination with abiraterone did not affect XPA mRNA expression in both LNCaP/ABI and 22RV1/ABI cell lines, indicating a post-transcriptional mechanism (Fig. 4A).

We then examined XPA protein stability after pausing with the protein synthesis inhibitor cycloheximide (CHX) together with or without IDA treatment. After CHX addition, XPA protein levels
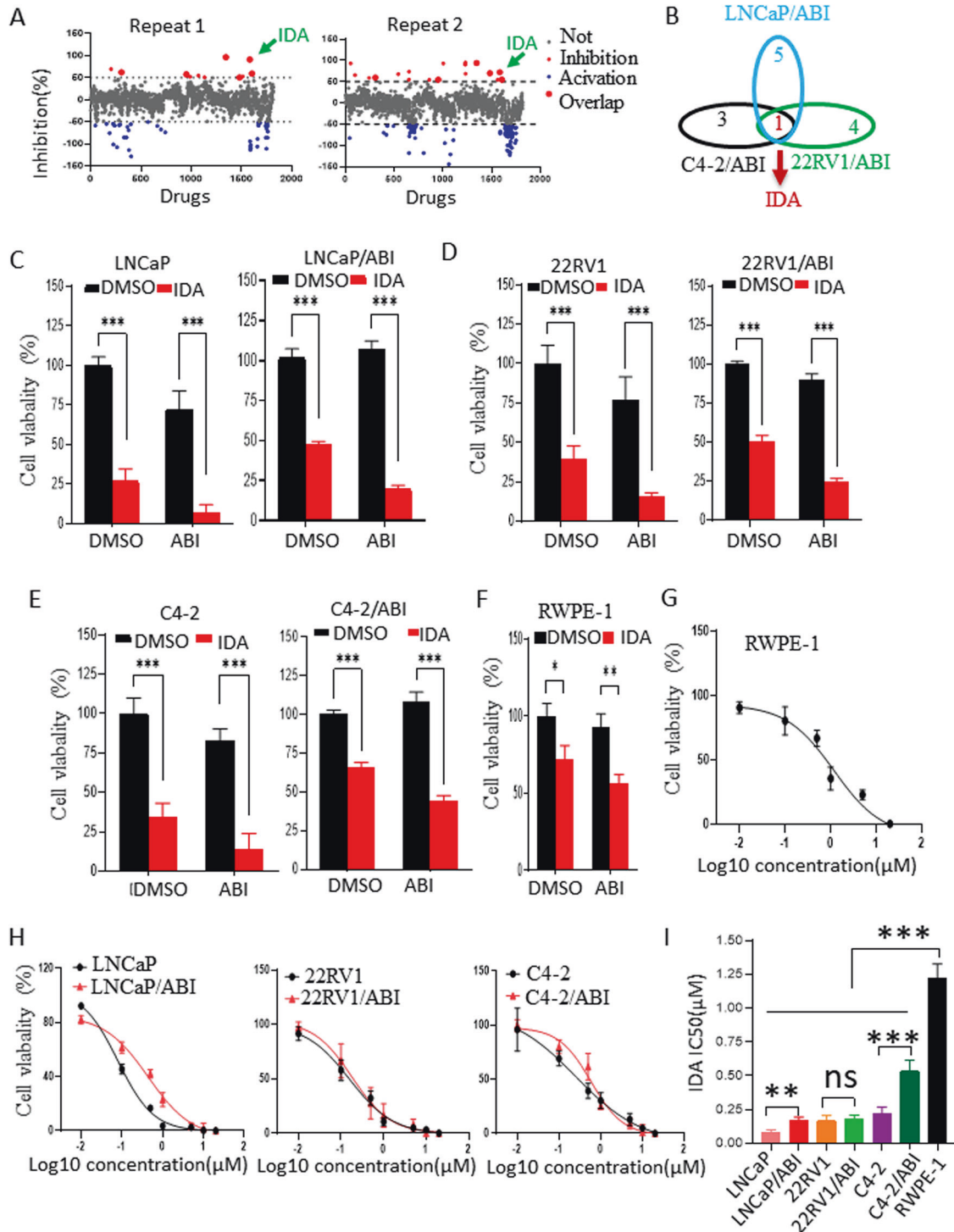
Fig. 1   Identification of drugs combats abiraterone resistance using a high-throughput assay. A LNCaP/ABI cells were seeded in 96 wells and treated for 24 h with an FDA-approved drug library, including 1815 drugs ($n = 2$). Cell viability was determined by CCK-8 assay. B C4-2/ABI and 22RV1/ABI cells were treated with the six drugs (i.g. Otilonium, Idarubicin, Auranofin, Sitafloxacin, Pyrvinium pamoate, and Erdafitinib) for 24 h. Cell viability was determined by CCK-8 assay. The Venn diagram indicates that IDA is a candidate drug for overcoming abiraterone resistance in LNCaP/ABI, C4-2/ABI, and 22RV1/ABI cells. C–F Abiraterone-resistant cell lines (LNCaP/ABI, 22RV1/ABI, and C4-2/ABI), the parental control cell lines (LNCaP, 22RV1, and C4-2), and RWPE-1 cells were treated with DMSO, IDA, ABI, or a combination of ABI and IDA for 24 h. Cell viability was determined by the CCK-8 assay ($n = 6$). G–I Abiraterone-resistant cell lines (LNCaP/ABI, 22RV1/ABI, and C4-2/ABI), the parental control cell lines (LNCaP, 22RV1, and C4-2), and RWPE-1 cells were treated with indicated concentration (i.g., 0 μM, 0.01 μM, 0.1 μM, 0.5 μM, 1 μM, 2 μM, 5 μM, 10 μM, 20 μM) in the presence of abiraterone (10 μM) for 24 h. Cell viability was determined by CCK-8 assay($n = 6$). IC_{50} was determined by dose-response curves. Data are presented as means ± s.e.m. The asterisks indicate significant differences (two-way ANOVA, $*p < 0.05$, $**p < 0.01$, $***p < 0.01$).
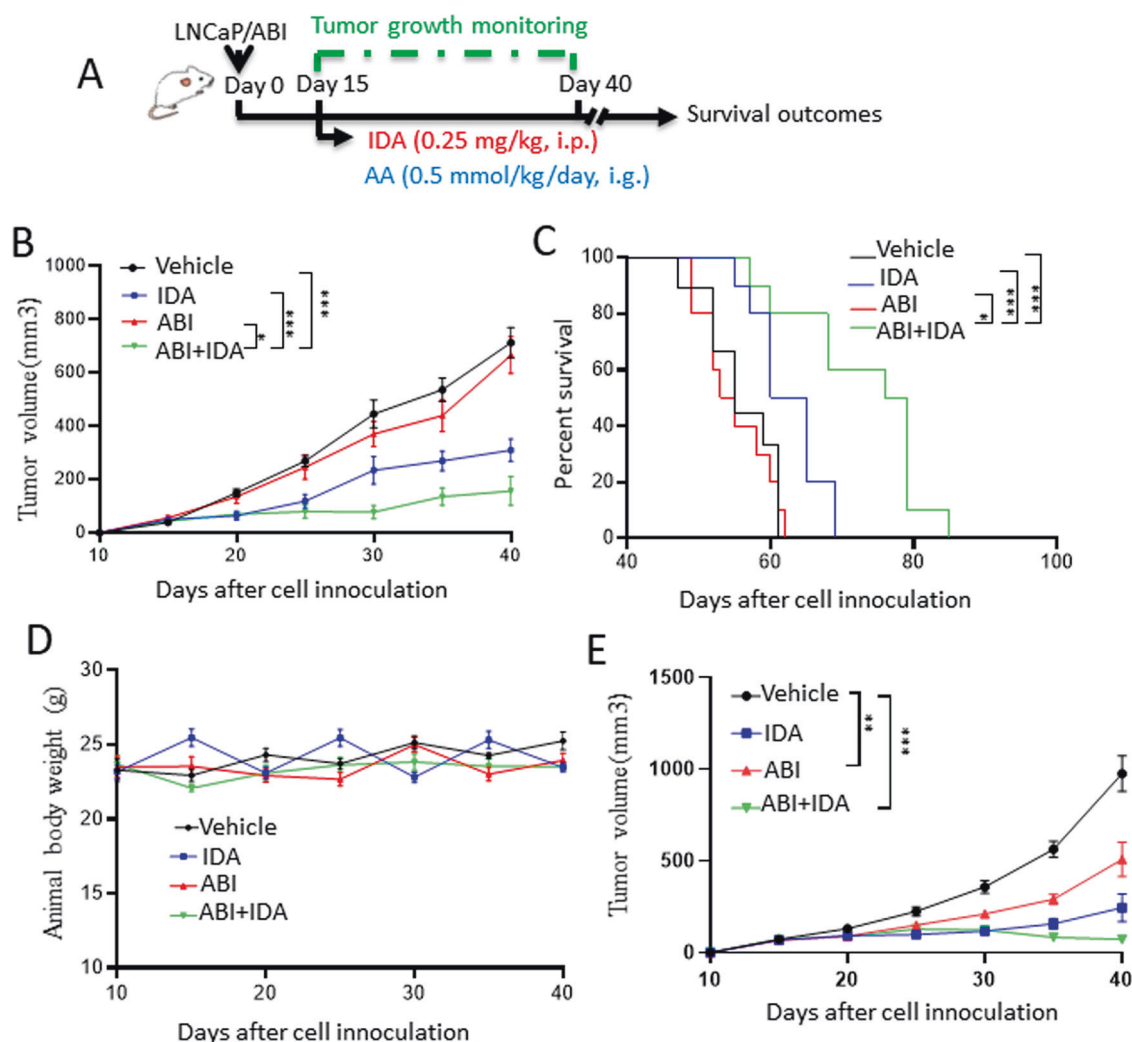
Fig. 2   IDA combats abiraterone resistance in vivo. A–D LNCaP/ABI cells were injected subcutaneously into the flanks of 8-week-old castrated male null mice. When tumor sizes reached about 50 mm³, mice were administered with the vehicle (10% DMSO plus 90% corn oil mixture as control, $n = 8$), IDA (0.25 mg/kg, i.p.), AA (0.5 mmol/kg, i.g.), and combination AA(0.5 mmol/kg, i.g.) and IDA(0.25 mg/kg) ($n = 10$, per group) (**A**). Tumor volume ($n = 10$, per group) (**B**), survival ($n = 10$, per group) (**C**), and body weight ($n = 10$, per group) (**D**) were monitored as indicated days. **E** LNCaP cells were injected subcutaneously into the flanks of 8-week-old castrated male null mice. Mice were treated as shown in Fig. 2A. Tumor volume was monitored as indicated days ($n = 7$, per group). Data are presented as means ± s.e.m. The statistical significance of tumor growth (**B**, **E**) and body weight (**D**) were measured by two-way ANOVA analysis. Statistical analysis for overall animal survival (**C**) was performed using and Log-rank (Mantel-Cox) test analysis, respectively. The asterisks indicate significant differences between the indicated groups (*$p < 0.05$, **$p < 0.01$, ***$p < 0.001$).

gradually decreased along with time, while IDA plus CHX treatment significantly enhanced the reduction of XPA protein levels (Fig. 4B, C). These data indicate that IDA treatment promoted XPA protein degradation.

Ubiquitin-proteasome and autophagy are the common processes for protein degradation [28]. We then determined if these two pathways were involved in IDA-induced XPA degradation. LNCaP/ABI and 22RV1/ABI cells were treated with the proteasome inhibitor MG132 and the autophagy inhibitor Chloroquine (CQ) with or without IDA addition. IDA-induced XPA protein reduction was completely blocked by the addition of MG132 or CQ in both cell lines (Fig. 4D). However, IDA treatment did not stimulate the autophagy pathway since LC3B biosynthesis and cleavage were not altered after IDA treatment (Fig. 4E). In contrast, IDA treatment largely enhanced the level of XPA ubiquitination in LNCaP/ABI cells (Fig. 4F). These data strongly suggested that IDA promotes XPA protein degradation mainly via the proteasome pathway but the role of the autophagy pathway. The mechanism underlying XPA protein homeostasis needs further investigation.

IDA/XPA also combats enzalutamide resistance in prostate cancer cells

Accumulated evidence indicates that abiraterone resistance crosstalks with ENZ resistance under certain circumstances by sharing a similar mechanism (e.g., AR reactivation [29, 30], DNA repair [18], AKT pathway inhibition [31, 32]). Therefore, we investigated whether IDA could overcome enzalutamide resistance. First, enzalutamide-resistant prostate cancer cells (LNCaP/ENZ) were injected into the nude mice. When the tumor size reached 50 mm³, the mice were randomly divided into four groups and administered vehicle, IDA, ENZ, or a combination of ENZ and IDA (Fig. 5A). Consistent with the effect of IDA on abiraterone resistance, IDA also or in combination with ENZ significantly inhibited ENZ-resistant tumor growth (Fig. 5B) and increased mouse survival (Fig. 5C). Body weight of mice treated with IDA alone or in combination with ENZ treatment did not display significant differentiation compared to those treated with ENZ alone and vehicle (Fig. S7). We also determined the effect of IDA treatment on parental cells. LNCaP-bearing mice were administered with vehicle,
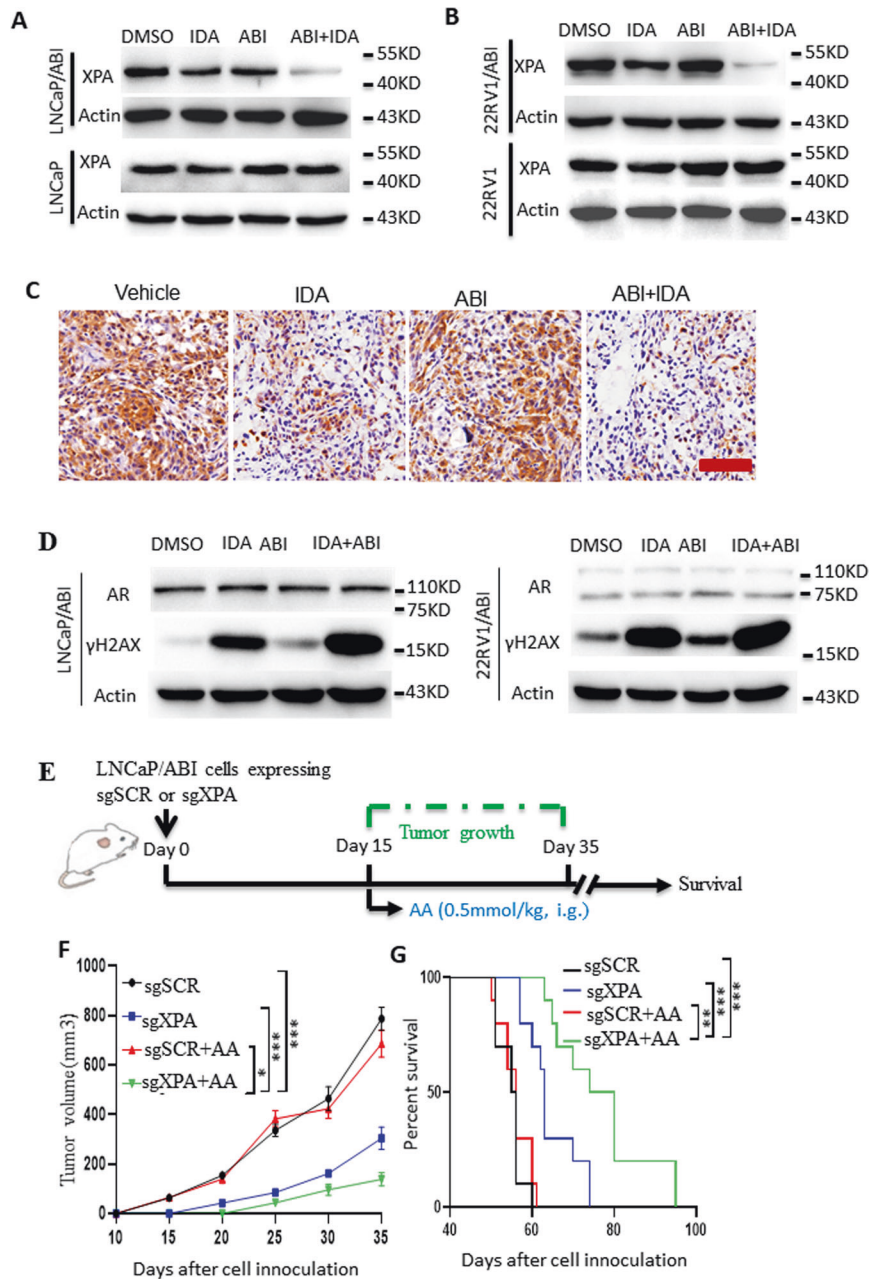
Fig. 3 XPA knockout combats the abiraterone resistance. A, B Abiraterone-resistant cells (LNCaP/ABI and 22RV1/ABI) and their parental control cells were treated with DMSO, ABI (10 μM), IDA (0.25 μM), and combination ABI with IDA. XPA expressions were determined by western blot. **C** XPA expression of tumor tissues from mice administered as shown in Fig. 2A was determined by IPC. Scale bar, 200 μm. **D** LNCaP/ABI and 22RV1/ABI cells were treated with DMSO, ABI (10 μM), IDA (0.25 μM), and combination ABI with IDA. Expressions of γH2AX and AR were determined by western blot. **E–G** LNCaP/ABI cells (1×10^6) were infected with lentivirus expressing sgSCR and sgXPA and then injected subcutaneously into the flank of 8-week-old male castrated mull mice. When tumor size reached about 50 mm^3, mice were administered with vehicle (10% DMSO plus 90% corn oil mixture as control, $n = 8$), AA (0.5 mmol/kg, i.g.), ($n = 10$, per group) (**E**). Tumor volume (**F**) and survival (**G**) were monitored as indicated days. Data are presented as means ± s.e.m. Statistical analysis for tumor growth and overall animal survival were performed using two-way ANOVA analysis (**F**) and Log-rank (Mantel-Cox) test analysis (**G**), respectively. The asterisks indicate significant differences between the indicated groups (*$p < 0.05$, ***$p < 0.001$).

IDA, ENZ, and a combination of IDA and ENZ, respectively. IDA alone and combined with ENZ treatment displayed antitumor activity in LNCaP-bearing mice (Fig. S8). These data indicated that IDA combats enzalutamide resistance.

We further assessed whether IDA affects AR expression and DNA damage in enzalutamide-resistant prostate cancer cells and their parental cell lines. Both IDA alone and in combination with ENZ significantly decreased the expression of XPA and enhanced the expression ofγH2AX compared with that observed in DMSO

and ENZ treatment in LNCaP/ENZ (Fig. 5D) and 22RV1/ENZ (Fig. 5E) cells. IDA alone and in combination with ENZ treatment displayed no effect on AR expression in LNCaP/ENZ and 22RV1/ENZ cells (Fig. 5D, E). These data indicate that IDA treatment enhanced DNA damage in ENZ-resistant cells.

We next determined whether ubiquitination and autophagy were involved in the IDA-induced decrease in XPA protein. Similarly, MG132 and CQ reversed the IDA-induced decrease in XPA protein levels in the presence of ENZ in LNCaP/ENZ and
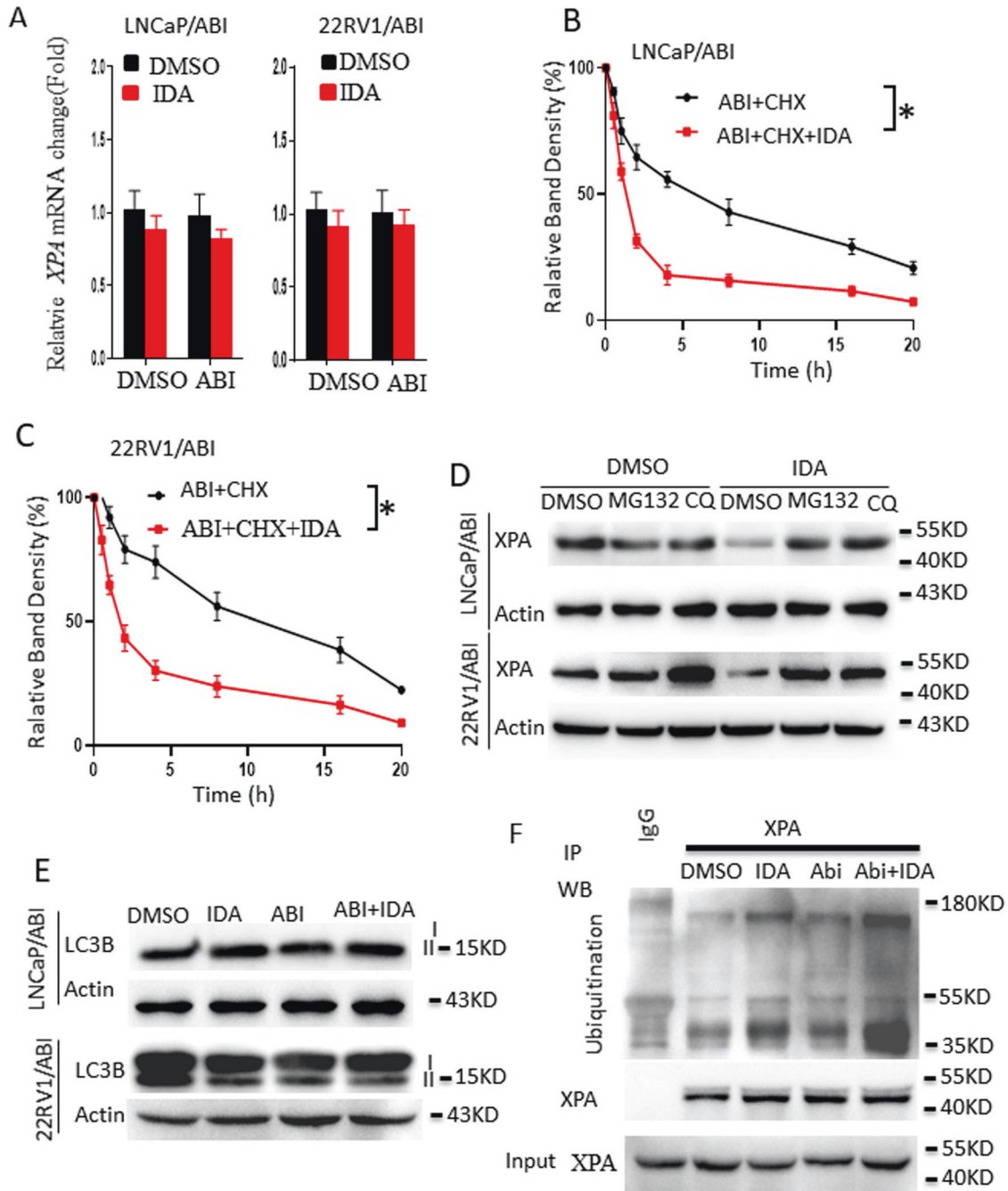
Y. Zhang et al.

Fig. 4 IDA regulates XPA protein levels by enhancing XPA protein degradation. A LNCaP/ABI and 22RV1/ABI cells were treated with DMSO, IDA (0.25 μM), ABI (10 μM), and a combination of IDA with ABI for 24 h. XPA mRNA expression was determined by Real-time PCR ($n = 4$). **B, C** LNCaP/ABI (**B**) and 22RV1/ABI (**C**) cells were treated with CHX (100 mM) alone or in a combination of IDA (0.25 μM) in the presence of ABI(10 μM) for the indicated periods. Band densities were determined by Image-J software, and the value at time-point 0 was set as 100%. **D** LNCaP/ABI and 22RV1/ABI cells were treated with DMSO, MG132, and CQ(30 μM) with or without IDA(0.25 μM) for 24 h. XPA protein levels were determined by western blot. **E** LNCaP/ABI and 22RV1/ABI cells were treated with DMSO, IDA(0.25 μM), ABI(10 μM), and a combination of IDA with ABI for 24 h. LC3B expressions were determined by western blot assay. **F** LNCaP/ABI cells were treated with DMSO, IDA(0.25 μM), ABI(10 μM), ABI plus IDA for 20 h. Proteasome inhibitor MG132 (1 μM) was included in the assay to protect the ubiquitinated protein from degradation. Ubiquitination of XPA was determined by western blot. Data are presented as means ± s.e.m. Statistical analysis was performed using two-way ANOVA analysis (Two-way ANOVA, *$p < 0.05$).

22RV1/ENZ cells (Fig. 5F). These data indicate that IDA decreases XPA protein levels and DNA damage by regulating XPA protein stability.

To assay the effect of XPA on ENZ-resistant prostate cancer cells in vivo, LNCaP/ENZ (1×10^6) expressing sgSCR or sgXPA were injected subcutaneously into the flanks of 8-week-old male castrated nude mice (Fig. 6A). The combination of XPA knockout with ENZ treatment significantly inhibited tumor growth (Fig. 6B) and prolonged mouse survival (Fig. 6C) compared to vehicle, sgSCR, or a combination of ENZ and sgSCR. These data indicate that IDA shares a similar mechanism for combating enzalutamide resistance in prostate cancer cells.
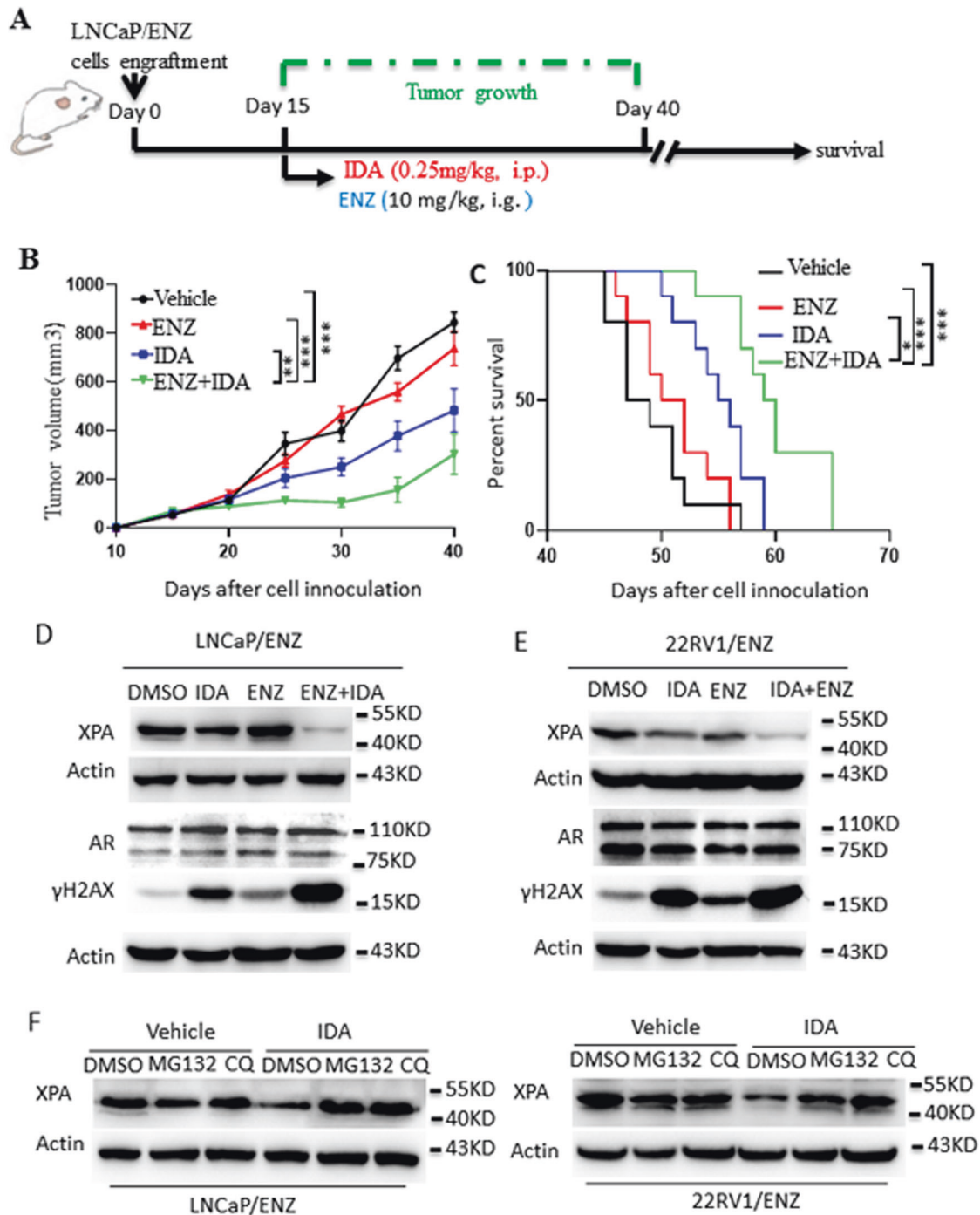
Fig. 5 IDA/XPA also combats enzalutamide resistance in prostate cancer cells. A–C LNCaP/ENZ cells were injected subcutaneously into the flanks of 8-week-old castrated male null mice. When tumor sizes reached ~50 mm³, mice were administered with the vehicle (10% DMSO plus 90% corn oil mixture as control, $n = 10$), IDA (0.25 mg/kg, i.p.), EZN (10 mg/kg, i.g.), and combination EZN (10 mg/kg) and IDA (0.25 mg/kg) (**A**). Tumor volume (**B**) and survival ($n = 10$, per group) (**C**) were monitored as indicated days. **D, E** LNCaP/ENZ (**D**) and 22RV1/ENZ(**E**) cells were treated with DMSO, IDA(0.25 μM), ENZ(10 μM), and a combination of ENZ with IDA for 24 h. XPA protein levels, γH2AX, and AR were determined by western blot. **F.** LNCaP/ENZ and 22RV1/ENZ cells were treated with DMSO, MG132(1 μM), and CQ(30 μM) with or without IDA(0.25 μM) for 24 h. XPA protein levels were determined by western blot. Data are presented as means ± s.e.m. Statistical analysis for tumor growth and overall animal survival were performed using two-way ANOVA analysis (**B**) and Log-rank (Mantel–Cox) test analysis (**C**), respectively. The asterisks indicate significant differences between the indicated groups (*$p < 0.05$, ***$p < 0.001$).

DISCUSSION

In this study, we found that IDA significantly overcame abiraterone and enzalutamide resistance in prostate cancer cells. IDA decreases XPA expression in a transcription-independent manner. XPA is a novel regulator of abiraterone and enzalutamide resistance in prostate cancer. XPA knockout inhibited abiraterone- and enzalutamide-resistant prostate cancer cell growth both in vitro and in vivo. In conclusion, IDA may be a promising candidate drug treatment for patients with abiraterone- and enzalutamide-resistant prostate cancer. Furthermore, XPA is
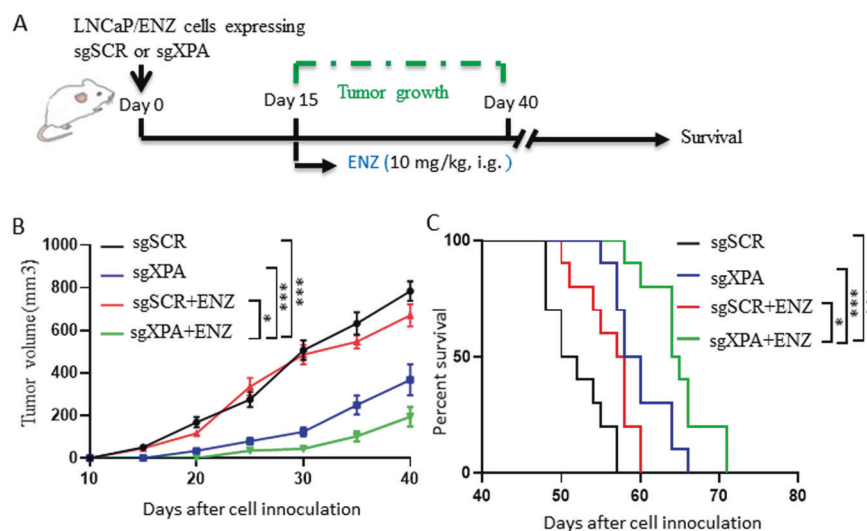
Fig. 6 XPA knockout combats the enzalutamide resistance. A–C LNCaP/ENZ cells (1 × 10^6) were infected with lentivirus expressing sgSCR and sgXPA and then injected subcutaneously into the flank of 8-week-old male castrated mull mice. When tumor size reached ~50 mm³, mice were administered with the vehicle (10% DMSO plus 90% corn oil mixture as control, $n = 10$), ENZ (10 mg/kg, i.g.) (**A**). Tumor volume ($n = 10$) (**B**) and survival ($n = 10$) (**C**) were monitored as indicated days. Data are presented as means ± s.e.m. Statistical analysis for tumor growth and overall animal survival were performed using two-way ANOVA analysis (**B**) and Log-rank (Mantel-Cox) test analysis (**C**), respectively. The asterisks indicate significant differences between the indicated groups (*$p < 0.05$, ***$p < 0.001$).

required for IDA-induced antitumor activity in abiraterone- and enzalutamide-resistant prostate cancer cells.

Although abiraterone and ENZ have been widely used for CRPC therapies, their clinical benefits are usually limited to 6 months due to resistance onset [7]. IDA, an anthracycline [33], is a mature clinical drug mainly used in leukemia treatment [24]. Recent studies have shown that IDA exhibits potent antitumor activity against several solid tumors such as hepatocellular carcinoma [25, 26]. In this study, we demonstrated that IDA inhibited the growth of abiraterone- and enzalutamide-resistant prostate cancer cells. Although previous studies have shown some toxic asocial effects with anthracycline treatment [34], we did not find significant side effects on mouse weight and tissues in this study. In addition, IDA treatment exhibited lower cytotoxicity in RWPE-1 normal cells than in prostate cancer cells. Thus, IDA may be a promising treatment option for patients with abiraterone- and enzalutamide -resistant prostate cancer.

The mechanisms underlying the progression of abiraterone and enzalutamide resistance remain unclear. It is widely accepted that AR reactivation [29, 30] and DNA repair [35] are involved in the advancement of resistance to second-generation androgen receptor antagonists. In addition, androgen deprivation regulated the DNA damage response via cross-talk between the AR pathway and DNA repair [18]. In this study, IDA treatment enhanced DNA damage but not AR expression, indicating that IDA treatment regulated DNA repair independent of the AR signaling pathway. Previous studies have demonstrated that combining abiraterone or enzalutamide with the DDR signaling pathway benefits patients with CRPC. Olaparib, a DNA repair inhibitor, in combination with abiraterone, significantly improved the survival of patients with CRPC compared to that observed with abiraterone treatment alone [36]. Similarly, the combination of ENZ with a DNA repair inhibitor effectively prolonged the survival of patients with CRPC compared to that observed with ENZ alone [37]. In this study, we found that IDA, in combination with AA, enhanced DNA damage by decreasing XPA protein levels and overcame the resistance of abiraterone and EZN, which is consistent with previous studies [36, 37].

Previous studies have demonstrated that XPA enhances chemo- and radiotherapy resistance in several cancers [20]. XPA is involved in several cisplatin-resistant cancers such as

gastric cancer [38], germ cell tumors [39], prostate cancer [40], and lung cancer [41]. In addition, XPA enhances temozolomide resistance in glioblastoma cells by promoting nucleotide excision repair [42]. Thus, XPA is a potential drug target for tumor therapy. In this study, we found that targeting XPA overcame abiraterone and EZN resistance in prostate cancer cells. XPA is a potential target for abiraterone- and EZN-resistant prostate cancer patients.

Furthermore, XPA expression is controlled by transcriptional regulation [43] and post-translational modification [20]. Previous studies have demonstrated that the circadian clock system [44] and hypoxia-inducible factor 1 alpha (HIF1α) [41] positively regulate the transcriptional expression of XPA. However, non-histone high-mobility group A1 (HMGA1) negatively regulates XPA expression [43]. We found that IDA treatment did not affect XPA mRNA expression in the present study. Therefore, we believe that IDA decreases XPA levels independent of the circadian clock system-, and HIF1a- and HMGA-induced the transcriptional regulation of XPA. XPA is also involved in other biological processes, including transcription [45]. In future studies, we will determine whether XPA mediates the progression of resistance independently of NER.

MATERIALS AND METHODS
Cell lines
Human prostate cancer cell lines LNCaP, 22RV1, C4-2 cells, and human prostate epithelial cell line RWPE-1 were obtained from ATCC (Manassas, VA, USA). LNCaP, 22RV1, and C4-2 cells were cultured in RPMI 1640 medium supplemented with 10% fetal bovine serum plus 100 U/ml penicillin/streptomycin and 2 mmol/l L-glutamine (Thermo-Fisher Scientific, Shanghai, China). RWPE-1 cells were cultured in a Keratinocyte-SFM medium (Invitrogen, CA, USA). All cell lines were authenticated by DNA Nineteen short tandem repeat (STR) at the Institute of Cancer Pathology Research Center at Jining Medical University. LNCaP and 22RV1 cell lines were authenticated on 1/2021, while C4-2 and RWPE-1 cell lines were authenticated on 9/2022. Mycoplasma presence was determined using the MycoSEQ™ Myco-plasma Detection Kit (catalog #4460623; Applied Biosystems).

Abiraterone and enzalutamide-resistant prostate cancer cells were generated as previously described [29]. Briefly, LNCaP, 22RV1, and C4-2 cells were cultured in a steroid-free medium (RPMI + 10% charcoal-stripped serum) for at least six months to establish ADT-resistant prostate

cancer cell lines. ADT-resistant prostate cancer cell lines were continuously treated with an increasing concentration of ABI or EZN from 0.5 μM to 10 μM for six months to establish ABI-resistant (i.e., LNCaP/ABI, 22RV1/ABI, and C4-2/ABI) and ENZ-resistant (i.e., LNCaP/ENZ and 22RV1/ENZ) sublines.

Reagents and antibodies
Antibodies against XPA (ab85914), and anti-ubiquitin (clone number: EPR8830; ab134953) were purchased from Abcam (Cambridge, MA, USA). Anti-γH2AX (clone number: 20E3; 9718) was obtained from cell signaling technology. Androgen receptor (clone number: PG-21; 06-680), Actin(clone number: AC-15; A5441), and LC3B (ABC432) antibodies were obtained from Sigma-Aldrich (St. Louis, MO). Protein A/G PLUS-Agarose (sc-2003) was obtained from Santa Cruz Biotech (Santa Cruz, CA). HRP-conjugated anti-rabbit IgG (light chain specific, 211-032-171) was ordered from Jackson immunoresearch lab (PA, USA). HRP-conjugated goat anti-mouse IgG and goat anti-rabbit IgG were obtained from Santa Cruz Biotech (Santa Cruz, CA, USA). Abiraterone acetate (AA, HY-75054), Abiraterone (HY-70013), Chloroquine (HY-17589A), MG-132 (Z-Leu-Leu-Leu-al) (HY-13259), Hoechst 33342 (HY-15559), and propidium iodide (PI) (HY-D0815) were obtained from MCE (New Jersey, NJ, USA).

Cell Counting Kit-8 cell viability assay
Cell viability was determined by CCK-8 Assay, as previously described [46]. Briefly, 1×10^5 cells were seeded in a 96-well culture plate. After 24 h incubation, the cell viability was determined using a CCK-8 (Beyotime, Shanghai, China) following the manufacturer's instruction. The absorbance at 450 nm was measured by CytExpert (Beckman Coulter, Brea, CA, USA).

High-throughput screening
The high-throughput screening was performed as described previously [47, 48]. Briefly, for the primary screen, LNCaP-ABI cells (1×10^4/well) were seeded in 96-well plates and treated with an FDA-Approved Drug Library at a final concentration of 1 μM for 24 h. Drug hits were determined by an inhibitory rate above 50% in a CCK-8 assay. LNCaP/ABI, 22RV1/ABI, and C4-2/ABI cells were treated with the drug hits on a secondary screen (Fig. S1A). The first and last rows of the assay plate were treated with the solvent DMSO. The positive (DMSO treatment with CCK-8 reagent) and the negative (DMSO treatment without CCK-8 reagent) were included in the assay (Fig. S1B). The equation to determine cell viability inhibition was as follows: inhibition % = $[(V_{DMSO} - V_{compound})/(V_{DMSO} - V_{neg})] \times 100$, where $V_{compound}$ denotes the values in compound-treated wells, V_{neg} indicates the value of DMSO treatment without CCK-8 reagent, and V_{DMSO} conveys the values of DMSO treatment with CCK-8 reagent. The drugs with an inhibitory rate over 50% in duplicate replications were regarded as the candidates

Cell death assay
Cell death was determined by Hoechst/propidium iodide (PI) staining assays as previously described [49, 50]. After drug treatment, cells were incubated in Hoechst (1 μg/ml) and PI(1 μg/ml) for 5 min. The microscopic images were taken using a Nikon Eclipse Ni (Nikon Instruments Inc., Melville, NY).

CRISPR/Cas9 screen
CRISPR/Cas9 screen was performed as previous studies [51, 52]. Briefly, LNCaP/ABI cells were infected with lentivirus bearing Human GeCKO Lentiviral sgRNA Library v2 (LentiCRISPR) (Addgene plasmid #1000000048). After selection with puromycin, cells were split into two groups. Ones were frozen at −80 °C as control. The others were injected subcutaneously into the flanks of 8-week-old castrated male nude mice. Mice administered with AA (0.5 mmol/kg/day). When tumors reached 1000 mm³, Mice were euthanized using CO_2 inhalation. Tumors were removed from mice. Genomic DNA were extracted form analysis cell pellets using a universal Genomic DNA Kit (Cwbio, Bejing, China). PCR was performed use a 2xGoldStar Best Mix kit according to manufacturer's protocol (Cwbio, Bejing, China). Primer sequences: sense 5′- AAT GGA CTA TCA TAT GCT TAC CGT AAC TTG AAA GTA TTT CG -3′, and antisense, 5′-AGC CAA TTC CCA CTC CTT TCA AGA CCT AGC-3′. PCR production was extracted from 2% agarose gel using a Gel Extraction Kit (Cwbio, Bejing, China) and subjected to next-generation sequencing (NGS) by a BGISEQ sequencing platform. Data were analyzed using MAGeCKFlute package [53]. Cumulative frequency was determined as previous studies [54].

Animal xenograft experiments
Tumor cells (1×10^6 cells/100 μl mixed 1:1 with Matrigel) were injected subcutaneously into the flanks of 8-week-old castrated male nude mice (Charles River, Beijing). Once tumor sizes reached about 50 mm³, mice were randomized for different treatments ($n = 7{\sim}10$), including IDA (0.25 mg/kg, i.p, twice weekly), AA (0.5 mmol/kg, i.g, five days per week) [55], and ENZ (10 mg/kg, i.g, five days per week) [56]. Vehicle (10% DMSO plus 90% corn oil mixture as control). Tumor diameter was blindly measured every five days using a digital caliper. Tumor volumes were calculated using the formula: [(length) × (width)²]/2 (V, mm³; L, mm; W, mm). Mice were euthanized with CO_2 inhalation at the end of the experiment. All animal procedures were performed according to the protocol approved by the institutional review committee of Jining Medical University for animal warfare (Ethical permission number: JNMC2021DW006). The animal experiments were carried out in compliance with the ARRIVE guidelines.

Western blotting and immunohistochemistry assays
Western blotting assay was performed as previously described [57, 58]. Briefly, treated cells were lysed with radioimmunoprecipitation assay (RIPA) buffer (Cell Signaling, Danvers, MA, USA), plugging a 1× protease inhibitor cocktail (Roche, Switzerland). Equal amounts of proteins were then subjected to sodium dodecyl sulfate-polyacrylamide gel electrophoresis (SDS-PAGE) and transferred onto a polyvinylidene fluoride membrane (Merck Millipore, UK). The membranes were incubated with primary antibodies (1:1000) at 4 °C overnight, followed by the peroxidase-conjugated secondary antibody (1:2000) for 1 h at room temperature. Immunoblots were visualized with ECL reagent (Beyotime, Shanghai, China).

Immunohistochemistry (IHC) staining assay was performed using an IHC kit according to the manufacturer's introduction (BOSTER, Wuhan, China). Briefly, paraffin-embedded tumor sections were deparaffinized and hydrated. Antigen retrieval was conducted in citric acid buffer (pH 6.0). After blocking for 30 min at room temperature, tissue sections were then incubated with primary antibodies at 4 °C overnight, followed by incubation with secondary antibodies for 1 h. Immunosignal visualization was performed with a DAPI-based reagent.

Real-time PCR
Total RNA was isolated using a Trizol reagent (ThermoFisher Scientific, Shanghai, China). The first strand of cDNA was synthesized using a 5× All-In-One Reverse Transcription Kit (ABM Company, Canada). The reverse transcript products (0.5 μl) were subjected to real-time PCR using an SYBR Green qPCR kit (ABM Company, Canada) using LightCycler® 480 instrument (ROCHE Diagnostic Spa, Mannheim, Germany). 18 S rRNA was used as an endogenous control. The relative expression level was calculated with the $2^{[-\Delta\Delta Ct]}$ approach and expressed as a fold-change. All data were normalized to the levels of 18 S rRNA expression. The primer sequences were designed as follows: 18 s rRNA sense 5′-GAG GAT GAG GTG GAA CGT GT-3′ and antisense 5′-GGA CCT GGC TGT ATT TTC CA-3′; XPA sense 5′-GAG TAT CGA GCG GAA GCG-3′ and antisense 5′-CTC CTG TGT CAA TTA TCT TTG GG-3′.

Cycloheximide assay
Cycloheximide Assay performed as previously described [59]. Briefly, LNCaP/ABI and 22RV1/ABI cells were treated with CHX (100 mM) alone or in a combination of IDA (0.25 μM) in the presence of ABI for the indicated periods. Band densities were determined by Image-J software, and the value at time-point 0 was set as 100%. The final density data were plotted against time using GraphPad Prism software.

Plasmid constructs, lentivirus package, and cell infection
Single guide RNA (sgRNA) anti-XPA was cloned into lentiCRISPR V2 (Addgene plasmid #52961) using BsmBI restriction enzyme sites [60]. Small hairpin interfering RNAs (shRNA) against XPA were cloned into PLKO.1-puro vector (Addgene Plasmid #8453) using AgeI/EcoRI restriction enzyme sites [61]. PAX2, pMD2.G (Addgene plasmid #12259-12260), and lenti-CRISPR V2 expressing sgRNA were co-transferred into 293 T cells. After 24 h incubation, the medium was changed to fresh medium and incubated for 24 h. Lentivirus-containing supernatants were collected and infected tumor cells. Stable expression clones were selected with puromycin (1 μg/ml). The sequence of sgRNA anti-XPA was listed as follows: sense, 5′-CAC CGT ACC TGC AGT TAT CAC AAG T-3′ and antisense, 5′-AAA CAC TTG TGA TAA CTG CAG GTA C-3′. The sequence of shRNA anti-XPA was listed as follows: sense,

5′-CAGAGATGCTGATGATAAA-3′ and antisense, 5′-TTTATCATCAGCATCTCT G-3′.

Ubiquitination detection assay

For ubiquitination detection, LNCaP-ABI cells were treated with DMSO, IDA, ABI, and ABI plus IDA for 20 h. Proteasome inhibitor MG132 (1 μM) was included in the assay to protect the ubiquitinated protein from degradation. Cells were lysed with NP-40 lysis buffer (50 mM Tris pH 7.4, 50 mM NaCl, 1% NP-40, 1x complete protease inhibitors) [62]. Protein lysates were incubated with XPA antibody/G-Agarose complexes for 8 h at 4 °C. The immunoprecipitant elutes were subjected to western blot assay with an anti-ubiquitin antibody followed by HRP-conjugated light chain specific anti-rabbit IgG.

Protein identification by Mass-Spectroscopy analysis

Total proteins were extracted using the SDT buffer (4% SDS, 100 mM Tris-HCl, 1 mM DTT, pH 7.6). After SDS-PAGE separation, proteins were digested in the gel. The desalted peptides were subjected to LC-MS/MS analysis using a Q Exactive Mass Spectrometer (Thermo Scientific, USA). Protein identification was conducted on the MaxQuant software (version 1.5.3.17) coupled with the UniProt database.

Data analysis

Data are presented as means ± SEM. Data were derived from at least three independent experiments. One-way variance analysis (ANOVA) was performed to determine the statistical significance among multiple groups. Differences in growth curves and survival were measured by two-way ANOVA and Log-rank (Mantel-Cox) test, respectively. Statistical analyses were performed using GraphPad Prism 8.0.2 software (GraphPad). $P < 0.05$ was considered statistically significant.

Reporting summary

Further information on research design is available in the Nature Research Reporting Summary linked to this article.

DATA AVAILABILITY

The data generated in this study are available within the article and its supplementary data files. Expression profile data analyzed of the CRISPR/ Cas9 screen in this study were obtained from Sequence Read Archive (SRA) at PRJNA780179. Protein Mass-Spectroscopy analyses were obtained from ProteomeX-change (PXD030905).

REFERENCES

1. Crawford ED, Petrylak D, Sartor O. Navigating the evolving therapeutic landscape in advanced prostate cancer. Urol Oncol. 2017;35S:S1–S13.
2. Fizazi K, Scher HI, Molina A, Logothetis CJ, Chi KN, Jones RJ, et al. Abiraterone acetate for treatment of metastatic castration-resistant prostate cancer: final overall survival analysis of the COU-AA-301 randomised, double-blind, placebo-controlled phase 3 study. Lancet Oncol. 2012;13:983–92.
3. Berruti A, Pia A, Terzolo M. Abiraterone and increased survival in metastatic prostate cancer. N Engl J Med. 2011;365:766.
4. Ryan CJ, Smith MR, Fizazi K, Saad F, Mulders PF, Sternberg CN, et al. Abiraterone acetate plus prednisone versus placebo plus prednisone in chemotherapy-naive men with metastatic castration-resistant prostate cancer (COU-AA-302): final overall survival analysis of a randomised, double-blind, placebo-controlled phase 3 study. Lancet Oncol. 2015;16:152–60.
5. de Bono JS, Logothetis CJ, Molina A, Fizazi K, North S, Chu L, et al. Abiraterone and increased survival in metastatic prostate cancer. N Engl J Med. 2011;364:1995–2005.
6. Scher HI, Fizazi K, Saad F, Taplin ME, Sternberg CN, Miller K, et al. Increased survival with enzalutamide in prostate cancer after chemotherapy. N Engl J Med. 2012;367:1187–97.
7. Buttigliero C, Tucci M, Bertaglia V, Vignani F, Bironzo P, Di Maio M, et al. Understanding and overcoming the mechanisms of primary and acquired resistance to abiraterone and enzalutamide in castration resistant prostate cancer. Cancer Treat Rev. 2015;41:884–92.
8. Caffo O, Veccia A, Maines F, Bonetta A, Spizzo G, Galligioni E. Potential value of rapid prostate-specific antigen decline in identifying primary resistance to abiraterone acetate and enzalutamide. Future Oncol. 2014;10:985–93.
9. Froehner M, Wirth MP. Enzalutamide in metastatic prostate cancer before chemotherapy. N Engl J Med. 2014;371:1755.
10. Wade CA, Kyprianou N. Profiling prostate cancer therapeutic resistance. Int J Mol Sci. 2018;19:904.
11. Swift SL, Lang SH, White H, Misso K, Kleijnen J, Quek RG. Effect of DNA damage response mutations on prostate cancer prognosis: a systematic review. Future Oncol. 2019;15:3283–303.
12. Grasso CS, Wu YM, Robinson DR, Cao X, Dhanasekaran SM, Khan AP, et al. The mutational landscape of lethal castration-resistant prostate cancer. Nature. 2012;487:239–43.
13. Robinson D, Van Allen EM, Wu YM, Schultz N, Lonigro RJ, Mosquera JM, et al. Integrative clinical genomics of advanced prostate cancer. Cell. 2015;162:454.
14. Hatano K, Nonomura N. Genomic profiling of prostate cancer: an updated review. World J Men's Health. 2022;40:368–79.
15. Taylor BS, Schultz N, Hieronymus H, Gopalan A, Xiao Y, Carver BS, et al. Integrative genomic profiling of human prostate cancer. Cancer Cell. 2010;18:11–22.
16. Armenia J, Wankowicz SAM, Liu D, Gao J, Kundra R, Reznik E, et al. The long tail of oncogenic drivers in prostate cancer. Nat Genet. 2018;50:645–51.
17. Kaelin WG Jr. The concept of synthetic lethality in the context of anticancer therapy. Nat Rev Cancer. 2005;5:689–98.
18. Polkinghorn WR, Parker JS, Lee MX, Kass EM, Spratt DE, Iaquinta PJ, et al. Androgen receptor signaling regulates DNA repair in prostate cancers. Cancer Discov. 2013;3:1245–53.
19. Goodwin JF, Schiewer MJ, Dean JL, Schrecengost RS, de Leeuw R, Han S, et al. A hormone-DNA repair circuit governs the response to genotoxic insult. Cancer Discov. 2013;3:1254–71.
20. Borszekova Pulzova L, Ward TA, Chovanec M. XPA: DNA repair protein of significant clinical importance. Int J Mol Sci. 2020;21:2182.
21. Asahina H, Kuraoka I, Shirakawa M, Morita EH, Miura N, Miyamoto I, et al. The XPA protein is a zinc metalloprotein with an ability to recognize various kinds of DNA damage. Mutat Res. 1994;315:229–37.
22. Orelli B, McClendon TB, Tsodikov OV, Ellenberger T, Niedernhofer LJ, Scharer OD. The XPA-binding domain of ERCC1 is required for nucleotide excision repair but not other DNA repair pathways. J Biol Chem. 2010;285:3705–12.
23. Fu X, Hu J, Han HY, Hua YJ, Zhou L, Shuai WD, et al. High expression of XPA confers poor prognosis for nasopharyngeal carcinoma patients treated with platinum-based chemoradiotherapy. Oncotarget. 2015;6:28478–90.
24. Iland HJ, Bradstock K, Supple SG, Catalano A, Collins M, Hertzberg M, et al. All-trans-retinoic acid, idarubicin, and IV arsenic trioxide as initial therapy in acute promyelocytic leukemia (APML4). Blood. 2012;120:1570–80.
25. Guiu B, Chevallier P, Assenat E, Barbier E, Merle P, Bouvier A, et al. Idarubicin-loaded beads for chemoembolization of hepatocellular carcinoma: the IDA-SPHERE II single-arm phase II trial. Radiology. 2019;291:801–8.
26. Boulin M, Hillon P, Cercueil JP, Bonnetain F, Dabakuyo S, Minello A, et al. Idarubicin-loaded beads for chemoembolisation of hepatocellular carcinoma: results of the IDASPHERE phase I trial. Aliment Pharm Ther. 2014;39:1301–13.
27. Abida W, Cyrta J, Heller G, Prandi D, Armenia J, Coleman I, et al. Genomic correlates of clinical outcome in advanced prostate cancer. Proc Natl Acad Sci USA. 2019;116:11428–36.
28. Wang Y, Le WD. Autophagy and ubiquitin-proteasome system. Adv Exp Med Biol. 2019;1206:527–50.
29. Simon I, Perales S, Casado-Medina L, Rodriguez-Martinez A, Garrido-Navas MDC, Puche-Sanz I, et al. Cross-resistance to abiraterone and enzalutamide in castration resistance prostate cancer cellular models is mediated by AR transcriptional reactivation. Cancers. 2021;13:1483.
30. Antonarakis ES, Lu C, Wang H, Luber B, Nakazawa M, Roeser JC, et al. AR-V7 and resistance to enzalutamide and abiraterone in prostate cancer. N Engl J Med. 2014;371:1028–38.
31. Adelaiye-Ogala R, Gryder BE, Nguyen YTM, Alilin AN, Grayson AR, Bajwa W, et al. Targeting the PI3K/AKT pathway overcomes enzalutamide resistance by inhibiting induction of the glucocorticoid receptor. Mol Cancer Ther. 2020;19:1436–47.
32. de Bono JS, De Giorgi U, Rodrigues DN, Massard C, Bracarda S, Font A, et al. Randomized phase II study evaluating Akt blockade with ipatasertib, in combination with abiraterone, in patients with metastatic prostate cancer with and without PTEN loss. Clin Cancer Res. 2019;25:928–36.
33. Betcher DL, Burnham N. Idarubicin. J Pediatr Oncol Nurs. 1990;7:117–20.
34. Horenstein MS, Vander Heide RS, L'Ecuyer TJ. Molecular basis of anthracycline-induced cardiotoxicity and its prevention. Mol Genet Metab. 2000;71:436–44.
35. Schmidt KT, Huitema ADR, Chau CH, Figg WD. Resistance to second-generation androgen receptor antagonists in prostate cancer. Nat Rev Urol. 2021;18:209–26.
36. Clarke N, Wiechno P, Alekseev B, Sala N, Jones R, Kocak I, et al. Olaparib combined with abiraterone in patients with metastatic castration-resistant prostate cancer: a randomised, double-blind, placebo-controlled, phase 2 trial. Lancet Oncol. 2018;19:975–86.
37. Reddy V, Iskander A, Hwang C, Divine G, Menon M, Barrack ER, et al. Castration-resistant prostate cancer: Androgen receptor inactivation induces telomere DNA

damage, and damage response inhibition leads to cell death. PLoS ONE. 2019;14:e0211090.

38. Pajuelo-Lozano N, Bargiela-Iparraguirre J, Dominguez G, Quiroga AG, Perona R, Sanchez-Perez I. XPA, XPC, and XPD modulate sensitivity in gastric cisplatin resistance cancer cells. Front Pharmacol. 2018;9:1197.

39. Cierna Z, Miskovska V, Roska J, Jurkovicova D, Pulzova LB, Sestakova Z, et al. Increased levels of XPA might be the basis of cisplatin resistance in germ cell tumours. BMC Cancer. 2020;20:17.

40. Cummings M, Higginbottom K, McGurk CJ, Wong OG, Koberle B, Oliver RT, et al. XPA versus ERCC1 as chemosensitising agents to cisplatin and mitomycin C in prostate cancer cells: role of ERCC1 in homologous recombination repair. Biochem Pharm. 2006;72:166–75.

41. Liu Y, Bernauer AM, Yingling CM, Belinsky SA. HIF1alpha regulated expression of XPA contributes to cisplatin resistance in lung cancer. Carcinogenesis. 2012;33:1187–92.

42. Dai W, Wu A, Li Y, Yu G, Yan X. XPA enhances temozolomide resistance of glioblastoma cells by promoting nucleotide excision repair. Cell Transplant. 2022;31:9636897221092778.

43. Adair JE, Kwon Y, Dement GA, Smerdon MJ, Reeves R. Inhibition of nucleotide excision repair by high mobility group protein HMGA1. J Biol Chem. 2005;280:32184–92.

44. Kang TH, Lindsey-Boltz LA, Reardon JT, Sancar A. Circadian control of XPA and excision repair of cisplatin-DNA damage by cryptochrome and HERC2 ubiquitin ligase. Proc Natl Acad Sci USA. 2010;107:4890–5.

45. Manandhar M, Lowery MG, Boulware KS, Lin KH, Lu Y, Wood RD. Transcriptional consequences of XPA disruption in human cell lines. DNA Repair. 2017;57:76–90.

46. Yamanaka K, Urano Y, Takabe W, Saito Y, Noguchi N. Induction of apoptosis and necroptosis by 24(S)-hydroxycholesterol is dependent on activity of acyl-CoA:-cholesterol acyltransferase 1. Cell Death Dis. 2014;5:e990.

47. Wang J, Huang Y, Wang S, Yang Y, He J, Li C, et al. Identification of active and inactive agonists/antagonists of estrogen receptor based on Tox21 10K compound library: Binomial analysis and structure alert. Ecotoxicol Environ Saf. 2021;214:112114.

48. Malo N, Hanley JA, Cerquozzi S, Pelletier J, Nadon R. Statistical practice in high-throughput screening data analysis. Nat Biotechnol. 2006;24:167–75.

49. Rogalska A, Marczak A, Gajek A, Szwed M, Sliwinska A, Drzewoski J, et al. Induction of apoptosis in human ovarian cancer cells by new anticancer compounds, epothilone A and B. Toxicol In Vitro. 2013;27:239–49.

50. Gasiorowski K, Brokos B, Kulma A, Ogorzalek A, Skorkowska K. A comparison of the methods applied to detect apoptosis in genotoxically-damaged lymphocytes cultured in the presence of four antimutagens. Cell Mol Biol Lett. 2001;6:141–59.

51. Huang K, Liu X, Li Y, Wang Q, Zhou J, Wang Y, et al. Genome-wide CRISPR-Cas9 screening identifies NF-kappaB/E2F6 responsible for EGFRvIII-associated temozolomide resistance in glioblastoma. Adv Sci. 2019;6:1900782.

52. Wei L, Lee D, Law CT, Zhang MS, Shen J, Chin DW, et al. Genome-wide CRISPR/Cas9 library screening identified PHGDH as a critical driver for Sorafenib resistance in HCC. Nat Commun. 2019;10:4681.

53. Wang B, Wang M, Zhang W, Xiao T, Chen CH, Wu A, et al. Integrative analysis of pooled CRISPR genetic screens using MAGeCKFlute. Nat Protoc. 2019;14:756–80.

54. Wu Y, Zhou L, Wang Z, Wang X, Zhang R, Zheng L, et al. Systematic screening for potential therapeutic targets in osteosarcoma through a kinome-wide CRISPR-Cas9 library. Cancer Biol Med. 2020;17:782–94.

55. Xiao L, Wang Y, Xu K, Hu H, Xu Z, Wu D, et al. Nuclear receptor LRH-1 functions to promote castration-resistant growth of prostate cancer via its promotion of intratumoral androgen biosynthesis. Cancer Res. 2018;78:2205–18.

56. Alajati A, D'Ambrosio M, Troiani M, Mosole S, Pellegrini L, Chen J, et al. CDCP1 overexpression drives prostate cancer progression and can be targeted in vivo. J Clin Investig. 2020;130:2435–50.

57. Li C, He C, Xu Y, Xu H, Tang Y, Chavan H, et al. Alternol eliminates excessive ATP production by disturbing Krebs cycle in prostate cancer. Prostate. 2019;79:628–639.

58. Li C, Jiang W, Hu Q, Li LC, Dong L, Chen R, et al. Enhancing DPYSL3 gene expression via a promoter-targeted small activating RNA approach suppresses cancer cell motility and metastasis. Oncotarget. 2016;7:22893–910.

59. Kim H, You S, Farris J, Foster LK, Foster DN. Post-transcriptional inactivation of p53 in immortalized murine embryo fibroblast cells. Oncogene. 2001;20:3306–10.

60. Sanjana NE, Shalem O, Zhang F. Improved vectors and genome-wide libraries for CRISPR screening. Nat Methods. 2014;11:783–4.

61. Li C, Xu H, Xiao L, Zhu H, Zhang G, Wei W, et al. CRMP4a suppresses cell motility by sequestering RhoA activity in prostate cancer cells. Cancer Biol Ther. 2018;19:1193–203.

62. Havel LS, Kline ER, Salgueiro AM, Marcus AI. Vimentin regulates lung cancer cell adhesion through a VAV2-Rac1 pathway to control focal adhesion kinase activity. Oncogene. 2015;34:1979–90.

ACKNOWLEDGEMENTS

AUTHOR CONTRIBUTIONS

Project administration and funding acquisition: CLLi, KY, and ZQ. Methodology: YZ, CYLi, SY, and CCH. Investigation: YZ, SY, WW, and SX. Validation and visualization: CLLi, and SW. Manuscript review and editing: CLLi, JL, and BL.

CONFLICT OF INTEREST

The authors declare no competing interests.

ETHICAL APPROVAL

All animal procedures were performed following the protocol approved by the institutional review committee of Jining Medical University for animal warfare (Ethical permission number: JNMC2021DW006). The study was carried out in compliance with the ARRIVE guidelines.

ADDITIONAL INFORMATION

Supplementary information The online version contains supplementary material available at https://doi.org/10.1038/s41419-022-05490-5.

Correspondence and requests for materials should be addressed to Kuo Yang or Changlin Li.

Reprints and permission information is available at http://www.nature.com/reprints

Publisher's note Springer Nature remains neutral with regard to jurisdictional claims in published maps and institutional affiliations.